Environment International 160 (2022) 107048

Contents lists available at ScienceDirect

Environment International

journal homepage: www.elsevier.com/locate/envint

Identification of ozone sensitivity for NO_2 and secondary HCHO based on MAX-DOAS measurements in northeast China

Jiexiao Xue [a], Ting Zhao [a], Yifu Luo [a], Congke Miao [a], Pinjie Su [a], Feng Liu [a], Guohui Zhang [a], Sida Qin [b], Youtao Song [a], Naishun Bu [a,c,*], Chengzhi Xing [d,*]

[a] School of Environmental Science, Liaoning University, Shenyang 110036, China
[b] Liaoning Science and Technology Center for Ecological and Environmental Protection, Shenyang 110161, China
[c] Key Laboratory of Wetland Ecology and Environment Research in Cold Regions of Heilongjiang Province, Harbin University, 150086, China
[d] Key Lab of Environmental Optics & Technology, Anhui Institute of Optics and Fine Mechanics, Hefei Institutes of Physical Science, Chinese Academy of Sciences, Hefei 230031, China

ARTICLE INFO

Handling Editor: Dr. Xavier Querol

Keywords:
MAX-DOAS
Formaldehyde
Secondary source
$HCHO/NO_2$
Ozone production sensitivity

ABSTRACT

In this study, tropospheric formaldehyde (HCHO) vertical column densities (VCDs) were measured using multi-axis differential optical absorption spectroscopy (MAX-DOAS) from January to November 2019 in Shenyang, Northeast China. The maximum HCHO VCD value appeared in the summer (1.74×10^{16} molec/cm^2), due to increased photo-oxidation of volatile organic compounds (VOCs). HCHO concentrations increased from 08:00 and peaked near 13:00, which was mainly attributed to the increased release of isoprene from plants and enhanced photolysis at noon. The HCHO VCDs observed by MAX-DOAS and OMI have a good correlation coefficient (R) of 0.78, and the contributions from primary and secondary HCHO sources were distinguished by the multi-linear regression model. The anthropogenic emissions showed unobvious seasonal variations, and the primary HCHO was relatively stable in Shenyang. Secondary HCHO contributed 82.62%, 83.90%, 78.90%, and 41.53% to the total measured ambient HCHO during the winter, spring, summer, and autumn, respectively. We also found a good correlation (R = 0.78) between enhanced vegetation index (EVI) and HCHO VCDs, indicating that the oxidation of biogenic volatile organic compounds (BVOCs) was the main source of HCHO. The ratio of secondary HCHO to nitrogen dioxide (NO_2) was used as the tracer to analyze O_3-NO_x-VOC sensitivities. We found that the VOC-limited, VOC-NO_x-limited, and NO_x-limited regimes made up 93.67%, 6.23%, 0.11% of the overall measurements, respectively. In addition, summertime ozone (O_3) sensitivity changed from VOC-limited in the morning to VOC-NO_x-limited in the afternoon. Therefore, this study offers information on HCHO sources and corresponding O_3 production sensitivities to support strategic management decisions.

1. Introduction

Formaldehyde (HCHO) can potentially influence tumor promotion within a specific concentration range (Agathokleous and Calabrese 2021; Bilal et al., 2021a) and is highly associated with lung, leukemia and nasopharyngeal cancer (Li et al., 2010; Tian et al., 2020). As one of the most abundant volatile organic compounds (VOCs) in the Earth's atmosphere (Ling et al., 2017; Friedfeld et al., 2002), HCHO plays a significant role in atmospheric photochemistry (Luecken et al., 2012; Hassan et al., 2018). For example, HCHO photolysis generates HO_x radical ($OH + HO_2$) (Ma et al., 2016), which strongly drive ozone (O_3) formation (Luecken et al., 2012). Recently, the HCHO and O_3 concentrations have been increasing in China, affecting the atmospheric oxidative capacity and resulting in photochemical smog (Sun et al., 2020; Li et al., 2021; Zhang et al., 2019). Therefore, an investigation into variation characteristics is greatly needed, to distinguish the sources of HCHO and better understand O_3-NO_x-VOC sensitivity to improve air quality.

Previous studies have used satellite measurements to estimate HCHO concentrations in different regions. For example, Bai et al. (2018) found

* Corresponding authors at: School of Environmental Science, Liaoning University, Shenyang 110036, China. Key Laboratory of Wetland Ecology and Environment Research in Cold Regions of Heilongjiang Province, Harbin University, 150086, China (N. Bu). Key Lab of Environmental Optics & Technology, Anhui Institute of Optics and Fine Mechanics, Hefei Institutes of Physical Science, Chinese Academy of Sciences, Hefei, 230031, China (C. Xing).
E-mail addresses: bunaishun@lnu.edu.cn (N. Bu), xingcz@aiofm.ac.cn (C. Xing).

https://doi.org/10.1016/j.envint.2021.107048
Received 14 August 2021; Received in revised form 11 December 2021; Accepted 13 December 2021
Available online 24 December 2021

that HCHO concentrations in agricultural and urban conditions were 121% and 125% higher than in background regions (anthropogenic VOC emissions were controlled) during 2005–2015, according to the Ozone Monitoring Instrument (OMI). Fan et al. (2021) also found that the human-induced sources of HCHO were higher compared to natural sources in urban areas, according to OMI measurements obtained between 2009 and 2018. Furthermore, biological contributions of HCHO emissions on O_3 formation exceeded anthropogenic sources in Shanghai during ozone pollution in 2013–2017, as observed by the Global Ozone Monitoring Experiment-2 (GOME-2) (Xu et al., 2021). Su et al. (2019) also reported that the averaged contributions of primary HCHO reached about 50.5% total HCHO concentrations at an industrial station in Nanjing, according to Ozone Mapping and Profiler Suite (OMPS) observations from 2015 to 2017. Unfortunately, satellite have low near-surface sensitivity and a coarse temporal resolution (Bilal et al., 2021b), which disqualifies them from HCHO diurnal cycles studies. Although *in situ* measurements have a higher temporal resolution and observation accuracy (Wang et al., 2019; Chen et al., 2014), they are usually limited to one location and lack vertical observation capabilities (Lui et al., 2017; Yang et al., 2019; Wang et al., 2010). Recently, a ground-based passive remote sensing technique was presented, with a high spatio-temporal resolution. This system, based upon multi-axis differential optical absorption spectroscopy (MAX-DOAS), can simultaneously measure multiple trace gases and analyze their chemical process (Khan et al., 2018). As a result, it provides a promising strategy to accurately investigate the photochemistry of HCHO and determining its contributions to O_3 formation (Xing et al., 2021; Benavent et al., 2019).

In addition, the total HCHO to nitrogen dioxide (NO_2) ratio in the atmosphere ($HCHO_{tot}/NO_2$) serves as an indicator of O_3-NO_x-VOC sensitivities, assuming that HCHO concentrations serve as proxies for VOC reactivity (Chi et al., 2018; Xing et al., 2017; Xu et al., 2021; Souri et al., 2020). Thus, HCHO sources are usually divided into primary emissions and secondary formations (Lui et al., 2017; Ho et al., 2012). Secondary HCHO is mainly formed through VOCs oxidation (i.e. isoprene) (Liu et al., 2018; Baek et al., 2014), and is positively correlated with peroxy radicals (RO_2) (Su et al., 2019; Chi et al., 2018). As a result, secondary HCHO is a reasonable agent to determine total VOC reactivity and precisely analyze the O_3-NO_x-VOC sensitivities. Therefore, wu can use the ratio of secondary HCHO and NO_2 ($HCHO_{sec}/NO_2$) to calculate O_3 sensitivity and avoid the O_3 sensitivity unreally inclining to NO_x-limited conditions and further misleading the air quality management.

Numerous O_3 sensitivity observations are available for HCHO/NO_2 based on satellite and ground data (Akshansha and Ramesh 2021; Hong et al. 2021; Souri et al. 2020; Wang et al. 2021; Jin et al. 2020). For example, Ryan et al. (2018) that reported the vast majority of high O_3 production episodes occurred under NO_x-limited conditions in Melbourne, Australia. Sakamoto et al. (2019) also showed that O_3 production was more sensitive to VOCs in the morning and evening, and it became more sensitive to NO_x during the afternoon in Tsukuba, Japan. Wang et al. (2016) revealed that in most urban and industrial regions in the eastern half of China, ozone production was limited by the VOCs. However, if primary HCHO had a relatively high contribution (>50%), then the corresponding HCHO/NO_2 would be overestimated, and some of the VOC-limited conditions would be misdiagnosed as NO_x-limited conditions (Liu et al. 2021). Thus, secondary HCHO may be more suitable for precisely analyzing O_3-NO_x-VOC sensitivity. VOCs from plants (i.e., isoprene) contribute significantly to secondary HCHO (Mahilang et al. 2021; Sindelarova et al. 2021), especially in high latitudes cities with long hours of sunshine and active photochemistry processes during the summer (Li et al., 2020a,b). These climate characteristics will aggravate VOCs from plant emissions, promoting HCHO and O_3 (Gao et al., 2020; Chen et al., 2018; Zhao et al., 2019). The highest hourly O_3 maximum values (exceeding 120 ppb) were found in southeastern France and north-western Italy during summer (Sicard et al., 2013). In Turin, which has some of the worst air quality in Europe, the limit values for O_3 were exceeded for 61 days in 2019 (Sicard et al., 2020). Therefore, it is of great significance to study O_3 sensitivity based on secondary HCHO, especially during different seasons in high latitudes cities, which possess unique climate characteristics.

Most VOCs produce HCHO through photolysis (Liu et al. 2017; Xing et al. 2020). Therefore, secondary HCHO is a more appropriate tracer to assess VOC activity (Liu et al. 2021; Su et al, 2019), and as a result, secondary HCHO may be more suitable for precisely analyzing O_3-NO_x-VOC sensitivities. In this study, we analyzed tropospheric HCHO sources from MAX-DOAS measurements. Section 2 provides detailed descriptions of the measurement instruments, data retrieval process, and the multiple linear regression models. Sections 3.1 and 3.2 present the temporal characteristics of the HCHO VCDs, which were compared with the ozone monitoring instrument (OMI) satellite observations. Sections 4.1 and 4.2 describe the contributions of primary emissions and secondary formations for HCHO VCDs, as well as O_3 formation sensitivity based on NO_2 and secondary HCHO data. Finally, the conclusions are presented in Section 5.

2. Measurements and methodology

2.1. Experimental setup

The MAX-DOAS instrument (2D-Envimes, Airyx, Heidelberg, Germany) was installed on the garret floor of the Huixing building in Liaoning University (41.23°N, 123.41°E) (Fig. 1), to provied continuous HCHO measurements from January to November 2019. The MAX-DOAS system composed of a telescope, two spectrometers, and a computer. The telescope and two spectrometers were stabilized at 20 °C, and the computer served as the control terminal. Scattered sunlight was collected by telescope and then guided into spectrometers through a prism reflector and quartz fiber. The telescope field of view was less than 0.3°, and the two spectrometers (Acton Spectrapro 300i Czerny-Turner optical spectrometer) were outfitted with a charge-coupled device detector camera (model DU 440-BU). The camera used 2048 pixels to measure the spectra in ultraviolet (UV) (300–460 nm) and visible (400–560 nm) wavelength ranges. The two spectrometers had a full-width half-maximum (FWHM) of 0.6 nm.

The full MAX-DOAS scan was divided into 11 elevation angles including 1, 2, 3, 4, 5, 6, 8, 10, 15, 30, and 90° (Xing et al., 2020). The exposure times for each measurement were automatically adjusted depending on the intensity of the received scattered sunlight, to ensure similar intensities for the measurements obtained at all elevations. In this study, the exposure time was denoted by the integration time, where the integration time = single exposure time scan number. Therefore, it did not result in saturation in the zenith direction and provided sufficient sensitivities in the off-axis directions. Each night, the instrument was set to collect dark current and offset spectra, which were subtracted from the measured spectra during the day.

We utilized the spectrometer in the UV range, where the spectrum measured at 90° was the reference spectrum for each sequence, to remove the effects of absorption in the stratosphere (Sinreich et al., 2005).

2.2. Spectral analysis

In this study, we utilized QDOAS spectral fitting software, which was developed by BIRA-IASB (http://uv–vis.aeronomie.be/software/QDOAS/, last access: 10 December 2019) to analyze the spectra measured by MAX-DOAS (Zara et al., 2018; Constantin et al., 2017; Michel et al., 2018; Hong et al., 2018; Xing et al., 2017). The fitted DOAS results consisted of differential slant column densities (DSCDs) of HCHO, which were calculated by subtracting the zenith reference spectra from the off-zenith spectra. Table 1 provides the detailed settings for the HCHO analysis, and an example DOAS spectral fitting of HCHO is shown in Fig. 2.

DSCDs with RMS values greater than 0.0025 (Javed et al., 2019) and

Fig. 1. Location of Shenyang.

Table 1
The DOAS retrieval settings for HCHO.

Parameter	Date source
NO_2	298 K, I_0* correction (SCD of 10^{17} molecules/cm^2); Vandaele, Hermans et al. (1998)
O_3	223 K, I_0* correction (SCD of 10^{20} molecules/cm^2); Serdyuchenko et al. (2014)
O_3	243 K, I_0* correction (SCD of 10^{20} molecules/cm^2); pre-orthogonalized; Serdyuchenko et al. (2014)
O_4	293 K; Thalman and Volkamer (2013)
BrO	223 K; Fleischmann et al. (2004)
HCHO	297 K; Meller and Moortgat (2000)
Ring	Calculated with QDOAS
Wavelength range	336.5–359 nm
Polynomial degree	Order5
Intensity offset	Constant

* Solar I_0 correction; Aliwell, Roozendael et al. (2002).

a solar zenith angle (SZA) larger than 80° were removed from the study (Xing et al., 2019).

The SCD was converted into a vertical column density (VCD) through the air mass factor (AMF) (Solomon and Schmeltekopf 1987), since the measured SCD depends on the absorption path in the atmosphere. Thus, AMF could be approximately calculated using the geometric method (AMFgeo) (Tack et al., 2021; Zara et al., 2021; Hönninger and Platt, 2002; Brinksma and Pinardi, 2008). Enhanced HCHO VCD retrievals were achieved using a more sophisticated AMF calculation, utilizing the Radiative transfer models (AMFrtm) (Wang et al, 2017b; Wagner et al., 2004; Gielen et al. 2014). AMFrtm could be approximated by AMFgeo, but only at altitudes between 2 and 4 km and SZA < 50° (Lamsal et al. 2017). Observations at low elevation angles could also result in large deviations from true tropospheric AMF and large errors could occur in the presence of high aerosol loads, even at high elevation angles (Brinksma and Pinardi, 2008; Bilal et al., 2017b; Bilal et al., 2019b). Therefore, using AMFgeo to convert SCD to VCD (VCDgeo) rather than AMFrtm (VCDrtm) greatly simplifies the retrieval approach and improves data quality, as the AMF conversion will be independent of some of the model parameter inputs (Lamsal et al., 2017). Halla et al. (2011) showed a high correlation between VCDgeo and VCDrtm (R^2 = 0.97), where VCDgeo was 8–12% lower than VCDrtm, assuming scaling error. In addition, Ibrahim et al. (2010) reported a geometric approximation method using AMF = 1/sin (α), where α is the elevation angle of MAX-DOAS. Thus, the tropospheric VCD (VCD_{Trop}) was represented by:

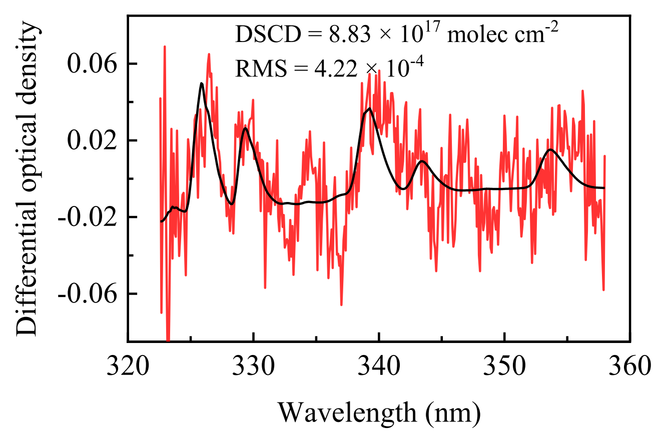

Fig. 2. Example of DOAS fitting results for HCHO; where the red and black curves indicate the fitted absorption structures and the derived absorption structures from the measured spectra, respectively, and spectra with an elevation angle of 8° and a SZA of 54.35° were selected. (For interpretation of the references to color in this figure legend, the reader is referred to the web version of this article.)

$$VCD_{TROP} = \frac{DSCD_{trop}}{\frac{1}{sin\alpha}} - 1. \quad (1)$$

In this study, we selected a 30° elevation angle to calculate the tropospheric HCHO VCDs. We then calculated the color index (CI), which was defined as the ratio of spectral intensities at 330 nm to 390 nm, to remove the cloud effects (Wagner et al., 2016). Subsequently, we filtered out data when the CI was less than 10% (Ryan et al., 2018), and the profiles for aerosol and trace gases were filtered out when the degree of freedom (DFS) was less than 1.0 and the retrieved relative errors were larger than 100% (Xing et al., 2021).

2.3. A multiple linear regression model

Carbon monoxide (CO) can be used as a tracer of primary HCHO (Friedfeld et al., 2002; Garcia et al., 2006) and odd oxygen O_x ($O_x = O_3 + NO_2$) can be used as an indicator of secondary HCHO (Wood et al., 2010), to distinguish the ground-surface HCHO sources. Thus, a multiple linear regression model was used to quantify the sources of HCHO according to the following equation:

$$[HCHO] = \beta_0 + \beta_1[CO] + \beta_2[O_x], \tag{2}$$

where β_0, β_1, and β_2 are model fitting coefficients, β_0 is the background level of HCHO, which cannot be divided into primary or secondary contributions, and [HCHO], [CO], and [O_x] represent the concentrations (in ppbv) of HCHO, CO, and O_x, respectively. The relative contributions of primary emissions, secondary formation, and background levels of HCHO to the ambient HCHO were calculated by the following equations:

$$P_{primary} = \frac{\beta_1[CO]}{[HCHO]} \times 100\%, \tag{3}$$

$$P_{Secondary} = \frac{\beta_2[O_x]}{[HCHO]} \times 100\%, \tag{4}$$

$$P_{Background} = \frac{\beta_0}{[HCHO]} \times 100\%, \tag{5}$$

where $P_{primary}$, $P_{secondary}$, and $P_{background}$ represent the contributions of primary emission, secondary formation, and background level to the total HCHO, respectively.

HCHO DSCDs was converted to ground surface HCHO mixing ratios (ppbv) using a simplified formula (Lee et al., 2008). Most studies have shown that atmospheric HCHO is mainly concentrated below 1 km in China (Li et al., 2013; Wang et al., 2017b; Chan et al., 2019). Therefore, the HCHO mixing ratios was calculated by:

$$M(ppbv) = \frac{1.25 \times DSCD(moleculesc/cm^2)}{B \times \Delta p(atm)} \tag{6}$$

where M represents the HCHO mixing ratio, B (2.688×10^{16}) is the unit conversion factor of DU to molecules /cm^2, $DSCD$ denotes the HCHO VCDs in the tropospheric, and $\triangle$p is the pressure difference between the surface and at 1 km (Ziemke et al., 2001).

2.4. Ancillary data

The level-3 monthly gridded enhanced vegetation index (EVI) data were derived from MODIS (https://giovanni.gsfc.nasa.gov/giovanni/, last access: 22 August 2020) with spatial resolution of 0.05° × 0.05° (Bilal et al., 2019a,b,c; 2017a,b). The pressure data was collected from Taoxian Airport (http://www.wunderground.com, last access: 18 August 2020) with a temporal resolution of 30 min, which was about 22.6 km away from our monitoring site. The CO, NO_2, and O_3 concentrations were obtained from one of the China National Environmental Monitoring Center (CNEMC) network stations, Lingdongjie monitoring station (41.84°N, 123.42°E) (http://www.cnemc.cn/, last access: 22 August 2020), which is about 1.5 km away from our monitoring site.

The OMI level-3 gridded HCHO product was derived from the NASA Goddard Earth Sciences Data and Information Services Center (GES-DISC) (https://disc.gsfc.nasa.gov/, last access: 18. Apr. 2020) with a spatial resolution of 13 × 24 km^2 (Boersma et al., 2011; Mhawish et al., 2021; Bilal et al., 2019a). The gridded OMI VCDs within 15 km of the measurement site (approximately averaged OMI pixel size) were averaged according to the monthly values. The overpass time of the OMI satellite over the Shenyang region was around 13:30 local time, and effective cloud fractions (CFs) and cloud top heights (CTHs) were taken from Tropospheric Emission Monitoring Internet Service (TEMIS) for OMI retrieval. CF values greater than 30% were excluded from the comparison.

3. Results

3.1. Overview of tropospheric HCHO

The ambient HCHO VCDs remained fluctuating within 15% around 1.00×10^{16} molec/cm^2 from January to April, and the HCHO VCDs increased twice, from April (9.2×10^{15} molec/cm^2) to August (19.01×10^{15} molec/cm^2) (Fig. 3a). This was possibly related to BVOCs oxidation, which produced HCHO when exposed to bright light, as the BVOC emission at the planetary level is 1150 Tg C/year (Calfapietra et al., 2013). BVOC emissions in China were 58.89 Tg in 2018, including 37.45 Tg isoprene. BVOC emissions increased between 2008 and 2018 at an annual rate of 2.03% (Li et al., 2020b) reaching the maximum level in August in northern China (Chen et al., 2020). The HCHO VCDs suddenly dropped from 19.01×10^{15} molec/cm^2 in August to 10.11×10^{15} molec/cm^2 in September, and this phenomenon was attributed to the decrease in isoprene emissions in early September (Ding et al., 2016a; Ding et al., 2016b; Chen et al., 2020).

In this study, the seasons were defined as spring (March, April, May), summer (June, July, August), autumn (September, October, November), and winter (January, February). The diurnal HCHO VCDs varied in 8.8×10^{15}–11.7×10^{15}, 9.13×10^{15}–11.3×10^{15}, and 8.21×10^{15}–10.1×10^{15} molec/cm^2, for winter, spring, and autumn, respectively (Fig. 3b). In summer, the HCHO concentrations increased from 08:00 (1.18×10^{16} molec/cm^2) and peaked at 13:00 (2.08×10^{16} molec/cm^2). Vehicle emissions are a significant source of HCHO during early morning rush hour (Li et al., 2014; Fan et al., 2021). The higher temperature and stronger solar radiation intensity at noontime increased the release of isoprene from plants (Jiang et al., 2019; Chen et al., 2020) and promoted the photo-oxidation of VOCs to produce HCHO (Li et al., 2020a,b).

3.2. Comparison with OMI HCHO data

The HCHO VCDs extracted from the MAX-DOAS measurements were compared with the OMI observations. For better comparison, the MAX-DOAS data were averaged from 12:00 to 14:00, around the time of the OMI satellite overpass (Cheng et al., 2019), and we found a good correlation with R of 0.764 between the MAX-DOAS HCHO VCDs and OMI HCHO VCDs (Fig. 4). However, OMI observations were on averaged 40% lower than MAX-DOAS measurements. These differences were attributed to the averaging effect of the OMI observations with large pixels, including the neighboring clean areas (Hong et al., 2018), as well as the aerosol shielding effect and coverage effect of clouds (Javed et al., 2019).

4. Discussion

4.1. Estimation sources of HCHO

The concentration of ambient HCHO depends on the primary emissions and the photo-oxidation of VOCs (Fan et al., 2021; Taguchi et al., 2021; Li et al., 2014). However, the quantitative evaluation of HCHO sources is usually incomplete. In this study, found the secondary HCHO accounted for 82.62%, 83.90%, 78.90% and 41.53 % of the emissions in winter, spring, summer and autumn, respectively. Secondary HCHO in spring (3.58 ppbv) and summer (6.30 ppbv) was significantly higher than in winter (2.96 ppbv) and autumn (1.53 ppbv). Furthermore, the

Fig. 3. (a) Monthly variations for tropospheric HCHO VCDs, (b) diurnal cycles of tropospheric HCHO VCDs, averaged for different seasons from January to November 2019. Note that the error bars indicate the fit coefficient error.

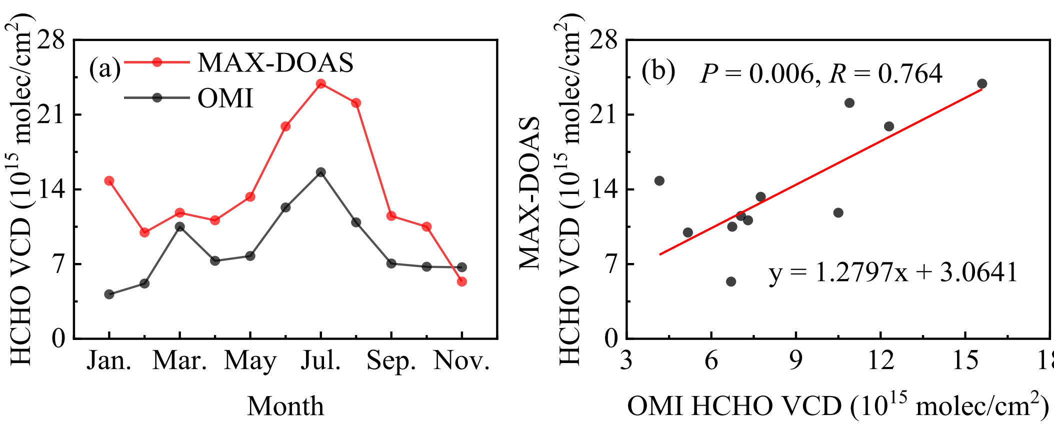

Fig. 4. Comparison of tropospheric MAX-DOAS HCHO VCDs and OMI HCHO VCDs. (a) time series of monthly averaged MAX-DOAS and OMI HCHO VCDs, and (b) the linear regression of the HCHO VCDs measured by MAX-DOAS and OMI.

enhanced vegetation index (EVI) was highly sensitive to vegetation growth, and resistant to the effects of dark soils and atmospheric noise (Nepita-Villanueva et al., 2019; Sun et al., 2021). Therefore, we used EVI as an indicator of this BVOC trend and we found the monthly averaged HCHO VCDs and EVI (Fig. 5) showed a significant correlation (R = 0.78). That indicates the photo-oxidation of BVOCs strongly contributed to ambient HCHO in Shenyang. Deciduous trees such as Populus alba × Populus berolinensis, Salix babylonica, Syringa oblata, and Ligustrum obtusifolium, mainly emitted isoprene, and their emission rates were 97.33, 17.71, 3.78, 0.13 μg·(g·h)$^{-1}$ in Shenyang, respectively (Shi et al., 2011) (Tables 2S–4S). However, Ma et al. (2019) obtained different results, showing that primary emission (i.e. Vehicle exhaust) was the main source of HCHO in August and September in Shenyang. This difference was attributed to the rapid development of industrialization and urbanization, which affected the precursors of HCHO. According to Shen Yang Statistics Bureau of China in 2019, the number of chemical industry plants and the use of natural gas increased by about 14% and 69% from 2017 to 2019, respectively. The increase in industry and natural gas contributed to the increase in VOC emissions (Khan et al., 2018), promoting the formation of secondary HCHO. As shown in Fig. 6b,

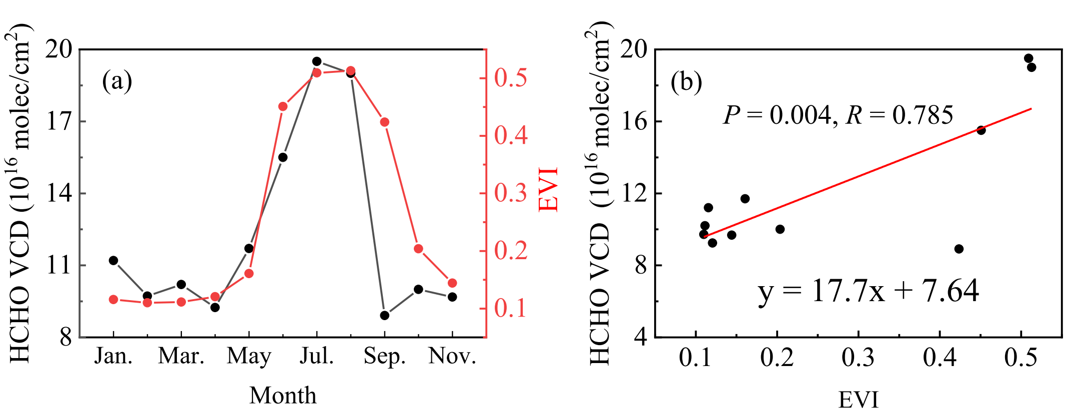

Fig. 5. Comparison of monthly averaged HCHO VCDs measured by MAX-DOAS and EVI data. (a) Time series of HCHO VCDs and EVI data. (b) Scatter plots for the HCHO VCDs and EVI data.

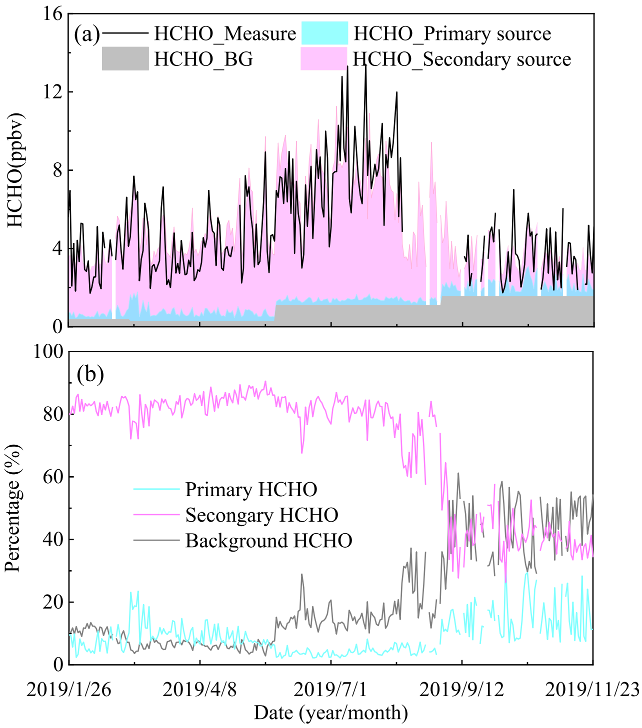

Fig. 6. The time series of the absolute (a) and relative (b) contributions of primary, secondary and background sources for ambient HCHO concentrations from January to November 2019 in Shenyang.

primary HCHO was relatively stable at a mean value of 0.41 ppbv, indicating anthropogenic emissions (i.e. wintertime coal combustion for heating) was an inconspicuous seasonal variation in Shenyang. The background levels of HCHO also significantly contribution (43.47%) to ambient HCHO levels during autumn, which was possibly regulation with CH_4 (Taguchi et al., 2021). CH_4 can be directly oxidized into HCHO and transported over long distance due to its long lifespan (Khan et al., 2018; Yang et al., 2019).

In this study, the contributions of secondary HCHO reached their maximum value between 12:00 and 14:00 in the summer. We defined this type of diurnal modality as a single peak type, as it created U-shape. The same HCHO variations during the day were also discovered in Houston-Galveston Airshed (Rappengluck et al., 2010), as well as Mexico (Lei et al., 2008), Shenzhen (Wang et al., 2017a) and Toyama (Taguchi et al., 2021). Table 2 shows detailed information regarding the sources and diurnal variations of HCHO in cities worldwide. The relative contributions of summertime secondary HCHO in Shenyang were within the range of the contributions of secondary HCHO in above cities. However, wintertime secondary HCHO in Shenyang was higher than in the previously mentioned cities.

4.2. O_3-NO_x-VOC sensitivities

Su et al. (2019) reported the total HCHO can be used as an indicator of VOC reactivity and used to analyze O_3 sensitivity, as secondary HCHO is the dominant source of HCHO. In this study, we used $HCHO_{tot}/NO_2$ and $HCHO_{sec}/NO_2$ to determine the sensitive types of O_3 formation type to illustrate how only using secondary HCHO can improve the accuracy of the calculated O_3 sensitivities. The sensitivities of O_3-NO_x-VOC were divided into the following three types: VOC-limited, VOC-NO_x-limited and NO_x-limited conditions (Gao et al., 2017). $HCHO/NO_2$ ratio <1 represents the production of O_3 reduction with diminishing level of VOCs (VOCs-limited), and $HCHO/NO_2$ ratio >2 represents NO_x-limited. When $1 < HCHO/NO_2$ ratio <2 characterizes a transition (VOC-NO_x-limited) regime where the momentary production of O_3 was affected by

Table 2
Overview of diurnal variations and sources of HCHO in cities worldwide.

Reference	Location	Measurement Date	Main source	Diurnal variation type (8:00–16:00)
Yang et al., 2019	Wuhan	2017	Primary (winter: 73%) Secondary (summer: 67%)	u-shaped Inverted u-shaped
Wang et al., 2017a	Shenzhen	2016	Secondary (winter: 82%) (spring: 80%) (summer: 91%) (autumn: 91%)	Inverted u-shaped
Li et al., 2014	Ziyang	2012 5 Dec. to 31 Dec.	Primary (winter: 60%)	u-shaped
Lin et al., 2012	New York	2009 15 Jul. to 3 Aug.	Secondary (summer: 70%)	Inverted u-shaped
Li et al., 2010	Beijing	2008 3 Jul.	Primary (summer: 76%)	u-shaped
Pang and Mu, 2006	Beijing	2005	Secondary (spring: 71%) (summer: 78%) (autumn: 73%)	Inverted u-shaped
Garcia et al., 2006	Mexico	2003 4 Apr. to 5 May	Secondary (spring: 58%)	Inverted u-shaped
Possanzini et al., 2002	Rome	1994–1997	Secondary (summer: 80–90%) Primary (winter: 65–70%)	Inverted u-shaped u-shaped
This work	Shenyang	2019 26 Jan. to 23 Nov.	Secondary (winter: 83%) (summer: 79%) (spring: 84%) (autumn: 42%)	– – Inverted u-shaped – –

both VOCs and NOx emissions (Duncan et al., 2010; Liu et al., 2017). Subsequently, we found a 12% difference in calculated O_3 sensitivity between using $HCHO_{tot}/NO_2$ and $HCHO_{sec}/NO_2$ in the summer (Table 3). This suggests that the influence of primary HCHO on total HCHO cannot be ignored, although the secondary HCHO accounted for 78.9% of total HCHO.

O_3 concentrations in spring and summer were significantly higher than in winter and autumn (Fig. 7), which is consistent with the HCHO concentration results (Fig. 3). Furthermore, O_3 sensitivities in spring and summer alternately occurred with VOC-NO_x-limited and VOC-limited, and they were NOx-limited in winter and autumn (Fig. 7). Gao et al.

Table 3
O_3 sensitivity types calculated using the $HCHO_{tot}/NO_2$ and $HCHO_{sec}/NO_2$ ratios.

Season	Spring		Summer		Autumn		Winter		Annual	
$HCHO/NO_2$	$HCHO_{tot}$	$HCHO_{sec}$	$HCHO_{tot}$	$HCHO_{sec}$	$HCHO_{tot}$	$HCHO_{sec}$	$HCHO_{tot}$	$HCHO_{sec}$	$HCHO_{tot}$	$HCHO_{sec}$
VOC-limited	93.34%	96.67%	70.74%	82.94%	99.09%	100.00%	100.00%	100.00%	88.61%	93.67%
VOC-NO_x-limited	6.51%	3.33%	27.59%	16.72%	0.91%	0.00%	0.00%	0.00%	10.83%	6.23%
NO_x-limited	0.15%	0.00%	1.67%	0.33%	0.00%	0.00%	0.00%	0.00%	0.56%	0.11%

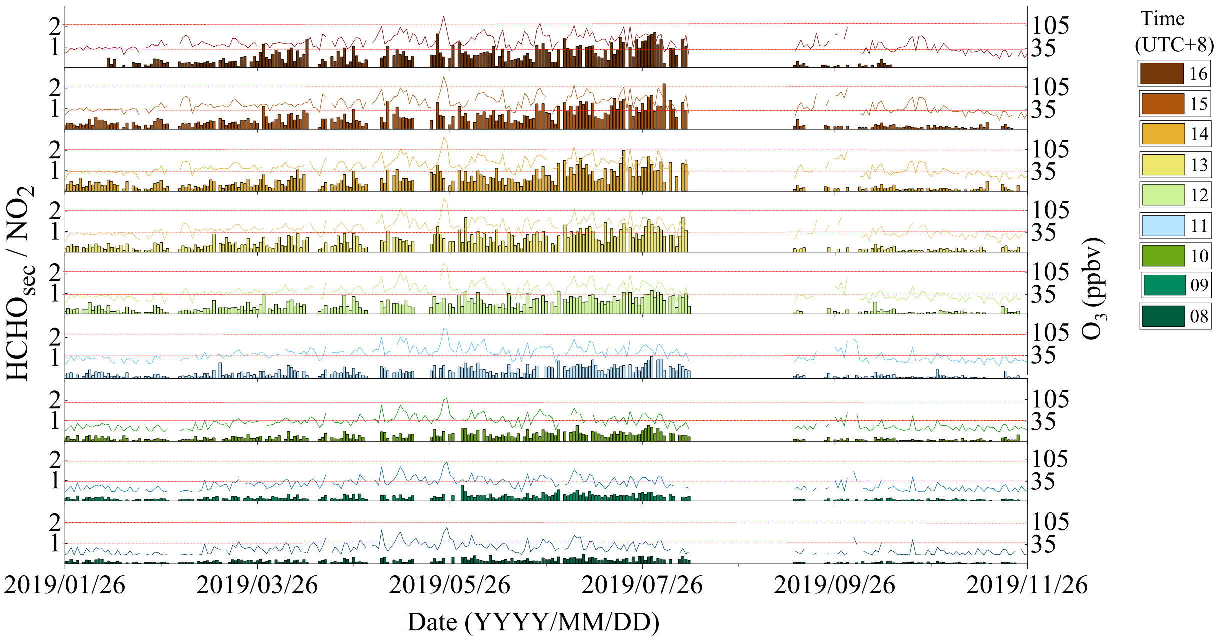

Fig. 7. Variations in $HCHO_{sec}/NO_2$ and O_3 between 08:00 and 16:00 from January to November 2019 (time as color information), where the column and curves indicate the $HCHO_{sec}/NO_2$ and O_3 concentrations, respectively.

(2020) also reported the surface O_3-NO_x-VOC sensitivity consisted of VOC-limited during spring, autumn and winter, while it was VOC-NO_x-limited during summertime in Liaoning, according to the $HCHO_{tot}/NO_2$ ratio. In this study, the hourly O_3 sensitivity production for VOC-limited, VOC-NO_x-limited and NO_x-limited conditions accounted for 93.67%, 6.23%, 0.11%, respectively. Thus, O_3 sensitivity during the summer generally showed a diurnal shift from the VOC-limited in the morning to the VOC-NO_x-limited in the afternoon. We also found the concentration of O_3 increase 20% between 12:00 and 13:00, and O_3 sensitivity correspondingly changed from VOC-limited to VOC-NO_x-limited (Fig. 7). Thesediurnal variation indicated that the identification of O_3 sensitivity regimes with high time resolution is needed to precisely control O_3 pollution.

China's government has issued a series of regulations and strategies to mitigate the high levels of air pollution. For example, the State Council of China issued the Air Pollution Prevention Action Plan (Huang et al., 2018; Li et al., 2020a) and the Win the Blue Sky Three-Year Action Plan in 2013 and 2018, which focused on reducing $PM_{2.5}$ concentrations (Wang 2021; Guo et al., 2020). Following these continuous emission control efforts, the annual mean $PM_{2.5}$ concentrations in 31 provincial capital cities reduced from 74 mg/m^3 to 39 mg/m^3 between 2013 and 2018 (http://english.mee.gov.cn/). Moreover, the annual average concentrations of PM_{10}, SO_2, NO_2, and CO decreased by 27.8%, 54.1%, 9.7%, and 28.2% in 74 key cities, respectively; however, O_3 showed a fluctuating 20.4% increase (Li et al., 2020a; Feng et al., 2019). Therefore, the amount of O_3 produced was strongly dependent on the ratio of VOCs and NO_x (Calfapietra et al., 2013). However, previous control strategies for O_3 have only focused on legislation-enforced control of NO_x emissions (Xu et al., 2021), and ignored the fact that higher O_3 concentrations still occur in VOC-limited regions (Nichol et al., 2020). Therefore, this study may serve as a guide for government agencies regarding the control policies of O_3 pollution based on HCHOsec/NO_2, and perhaps avoid some of the VOC-limited conditions that can be misdiagnosed as NO_x-limited conditions when using $HCHO_{tot}/NO_2$.

5. Conclusions

The primary emissions of HCHO were relatively stable due to unnoticeable seasonal anthropogenic emissions, and photo-oxidation of BVOCs was an important source of HCHO. Therefore, the $HCHO_{sec}/NO_2$ ratio can be used as a reference value to infer O_3-VOC-NO_x sensitivities. We found that the VOC-limited regime was 93.67% from 8:00 to 16:00 during the study period. The sensitivities of O_3-VOC-NOx in the summer typically showed a diurnal shift from VOC-limited in the morning to VOC-NOx-limited in the afternoon. These results showed that the government needs to control the precursor emissions of O_3 differently during different periods, according to the $HCHO_{sec}/NO_2$ ratio, to control the formation of O_3.

O_3 concentrations have increased significantly worldwide, and O_3 that is formed in cities is carried downwind to non-urban areas through long-range transport (Paoletti et al., 2014). Therefore, it is necessary to use accurate tracer gases when calculating O_3 sensitivities and the results from this study can serve as a reference for future regional-scale collaborations on air quality management.

CRediT authorship contribution statement

Jiexiao Xue: Conceptualization, Methodology, Investigation, Visualization, Formal analysis, Writing – original draft. **Ting Zhao:** Investigation, Formal analysis. **Yifu Luo:** Methodology, Investigation. **Congke Miao:** Investigation, Formal analysis. **Pinjie Su:** Investigation, Writing – review & editing. **Feng Liu:** Investigation, Formal analysis. **Guohui Zhang:** Conceptualization, Investigation. **Sida Qin:** Methodology, Formal analysis. **Youtao Song:** Methodology, Investigation. **Naishun Bu:** Conceptualization, Investigation, Supervision, Writing – review & editing, Funding acquisition. **Chengzhi Xing:** Conceptualization, Resources, Writing – review & editing, Funding acquisition.

Declaration of Competing Interest

The authors declare that they have no known competing financial interests or personal relationships that could have appeared to influence the work reported in this paper.

Acknowledgments

This work was supported by the National Science Foundation of China [grant numbers 31972522], Liaoning Revitalization Talents Program [grant numbers XLYC2007032], National Key Research and Development Project of China [grant numbers 2018YFC1801200], Major Science and Technology Project of Liaoning Province [grant numbers 2019JH1/10300001], and the Scientific Research Fund of Liaoning Provincial Education Department [grant numbers LQN202003], and the Open Research Fund of Key Laboratory of Wetland Ecology and Environment Research in Cold Regions of Heilongjiang Province [grant numbers 201903], and the Presidential Foundation of the Hefei Institutes of Physical Science, Chinese Academy Sciences, China [grant numbers YZJJ2021QN06], and the Research Fund Program of Guangdong-Hongkong-Macau Joint Laboratory of Collaborative Innovation for Environmental Quality [grant numbers GHML2021-102], and the National Key Research and Development Program of China [grant numbers 2017YFC0212500]. We thank the Belgian Institute for Space Aeronomy (BIRA-IASB), Brussels, Belgium, for their freely accessible QDOAS software (http://uv-vis.aeronomie.be/software/QDOAS/). We would like to acknowledge the NASA for providing open access data for OMI HCHO VCD and EVI (https://disc.gsfc.nasa.gov/). We do appreciate the CNEMC network stations for CO, NO_2, and O_3 concentrations data (http://www.cnemc.cn/). We thank LetPub (www.letpub.com) for its linguistic assistance during the preparation of this manuscript.

Appendix A. Supplementary material

Supplementary data to this article can be found online at https://doi.org/10.1016/j.envint.2021.107048.

References

Agathokleous, E., Calabrese, E.J., 2021. Formaldehyde: Another hormesis-inducing chemical. Environ. Res. 199 https://doi.org/10.1016/J.ENVRES.2021.111395.

Akshansha, C., Ramesh, P.S., 2021. Effect of Lockdown on HCHO and Trace Gases over India during March 2020. Aerosol Air Qual. Res. 21 https://doi.org/10.4209/aaqr.2020.07.0445.

Aliwell, S.R., Van Roozendael, M., Johnston, P.V., Richter, A., Wagner, T., Arlander, D. W., Burrows, J.P., Fish, D.J., Jones, R.L., Tørnkvist, K.K., Lambert, J.-C., Pfeilsticker, K., Pundt, I., 2002. Analysis for bro in zenith-sky spectra: an intercomparison exercise for analysis improvement. J. Geophys. Res.: Atmos. 107 (D14) https://doi.org/10.1029/2001JD000329.

Baek, K.H., Kim, J.H., Park, R.J., Chance, K., Kurosu, T.P., 2014. Validation of OMI HCHO data and its analysis over Asia. Sci. Total Environ. 490, 93–105. https://doi.org/10.1016/j.scitotenv.2014.04.108.

Bai, J., Leeuw, G.D., Ronald, V.D.A., Smedt, I.D., Theys, N., Roozendael, M.V., Sogacheva, L., Chai, W.H., 2018. Variations and photochemical transformations of atmospheric constituents in north china. Atmos. Environ. 189, 213–226. https://doi.org/10.1016/j.atmosenv.2018.07.004.

Benavent, N., Garcia-Nieto, D., Wang, S., Saiz-Lopez, A., 2019. MAX-DOAS measurements and vertical profiles of glyoxal and formaldehyde in Madrid, Spain. Atmos. Environ. 199, 357–367. https://doi.org/10.1016/j.atmosenv.2018.11.047.

Boersma, K.F., Eskes, H.J., Dirksen, R.J., Van Der A, R.J., Veefkind, J.P., Stammes, P., Huijnen, V., Kleipool, Q.L., Sneep, M., Claas, J., Leitao, J., Richter, A., Zhou, Y., Brunner, D., 2011. An improved tropospheric NO2 column retrieval algorithm for the Ozone Monitoring Instrument. Atmos. Meas. Tech. 4, 1905–1928. https://doi.org/10.5194/amt-4-1905-2011.

Bilal, M., Mhawish, A., Nichol, J.E., Qiu, Z.F., Nazeer, M., Ali, M.A., Leeuw, G., Levy, R. C., Wang, Y., Chen, Y., Wang, L.C., Shi, Y., Bleiweiss, M.P., Mazhar, U., Atique, L., Ke, S., 2021a. Air pollution scenario over Pakistan: Characterization and ranking of extremely polluted cities using long-term concentrations of aerosols and trace gases. Remote Sens. Environ. 264 https://doi.org/10.1016/J.RSE.2021.112617.

Bilal, M., Qiu, Z., Nichol, J.E., Mhawish, A., Ali, M.A., Khedher, K.M., Leeuw, G., Yu, W., Tiwari, P., Nazeer, M., Bleiweiss, M.P., 2021b. Uncertainty in aqua-modis aerosol retrieval algorithms during covid-19 lockdown. IEEE Geosci. Remote Sens. Lett. 1 (1), 5. https://doi.org/10.1109/LGRS.2021.3077189.

Bilal, M., Nazeer, M., Nichol, J.E., Bleiweiss, M.P., Qiu, Z., Jäkel, E., Campbell, J.R., Atique, L., Huang, X., Lolli, S., 2019a. A Simplified and Robust Surface Reflectance Estimation Method (SREM) for Use over Diverse Land Surfaces Using Multi-Sensor Data. Remote Sens. 11 (11) https://doi.org/10.3390/rs11111344.

Bilal, M., Nazeer, M., Nichol, J., Qiu, Z., Wang, L., Bleiweiss, M., Bleiweiss, M., Shen, X., Campbell, J., Lolli, S., 2019b. Evaluation of terra-modis c6 and c6.1 aerosol products against Beijing, Xianghe, and Xinglong aeronet sites in china during 2004–2014. Remote Sens. 11 (5) https://doi.org/10.3390/rs11050486.

Bilal, M., Nichol, J.E., Wang, L., 2017a. New customized methods for improvement of the MODIS C6 Dark Target and Deep Blue merged aerosol product. Remote Sens. Environ. 197, 115–124. https://doi.org/10.1016/j.rse.2017.05.028.

Bilal, M., Nazeer, M., Nichol, J.E., 2017b. Validation of MODIS and VIIRS derived aerosol optical depth over complex coastal waters. Atmos. Res. 186, 43–50. https://doi.org/10.1016/j.atmosres.2016.11.009.

Bilal, M., Nichol, J.E., Nazeer, M., Shi, Y., Wang, L., Kumar, K.R., Ho, H.C., Mazhar, U., Bleiweiss, M.P., Qiu, Z., Khedher, K.M., Lolli, S., 2019c. Characteristics of Fine Particulate Matter ($PM_{2.5}$) over Urban, Suburban, and Rural Areas of Hong Kong. Atmosphere 10 (9). https://doi.org/10.3390/atmos10090496.

Brinksma, E.J., Pinardi, G., Volten, H., Braak, R., Richter, A., Schönhardt, A., van Roozendael, M., Fayt, C., Hermans, C., Dirksen, R.J., Vlemmix, T., Berkhout, A.J.C., Swart, D.P.J., Ötjen, H., Wittrock, F., Wagner, T., Ibrahim, O.W., de Leeuw, G.M., Moerman, R.L., Curier, E.A., Celarier, W.H., Cede, A., Knap, J.P., Veefkind, H.J., Eskes, M., Allaart, R., Rothe, A., Piters, J.M., Levelt, P.F., 2008. The 2005 and 2006 DANDELIONS NO_2 and aerosol intercomparison campaigns. J. Geophys. Res.: Atmos. 113 (D16) https://doi.org/10.1029/2007JD008808.

Calfapietra, C., Fares, S., Manes, F., Morani, A., Sgrigna, G., Loreto, F., 2013. Role of Biogenic Volatile Organic Compounds (BVOC) emitted by urban trees on ozone concentration in cities: A review. Environ. Pollut. 183, 71–80. https://doi.org/10.1016/j.envpol.2013.03.012.

Chan, K., Wang, Z., Ding, A., Heue, K., Wenig, M., 2019. MAX-DOAS measurements of tropospheric NO_2 and HCHO in Nanjing and a comparison to ozone monitoring instrument observations. Atmos. Chem. Phys. 19 (15), 10051–10071. https://doi.org/10.5194/acp-19-10051-2019.

Chen, J., Tang, J., Yu, X., 2020. Environmental and physiological controls on diurnal and seasonal patterns of biogenic volatile organic compound emissions from five dominant woody species under field conditions. Environ. Pollut. 259 https://doi.org/10.1016/j.envpol.2020.113955.

Chen, W., Shao, M., Lu, S.H., Wang, M., Zeng, L.M., Yuan, B., Liu, Y., 2014. Understanding primary and secondary sources of ambient carbonyl compounds in Beijing using the pmf model. Atmos. Chem. Phys. 14, 3047–3062. https://doi.org/10.5194/acp-14-3047-2014.

Chen, W., Zhang, S., Tong, Q., Zhang, X., Zhao, H., Ma, S., Xiu, A., He, Y., 2018. Regional Characteristics and Causes of Haze Events in Northeast China. Chinese Geogr. Sci. 28, 836–850. https://doi.org/10.1007/s11769-018-0965-3.

Cheng, S., Ma, J., Cheng, W., Yan, P., Zhou, H., Zhou, L., Yang, P., 2019. Tropospheric NO_2 vertical column densities retrieved from ground-based MAX-DOAS measurements at Shangdianzi regional atmospheric background station in China. J. Environ. Sci. 80, 186–196. https://doi.org/10.1016/j.jes.2018.12.012.

Chi, X., Liu, C., Xie, Z., Fan, G., Wang, Y., He, P., Fan, S., Hong, Q., Wang, Z., Yu, X., Yue, F., Duan, J., Zhang, P., Liu, J., 2018. Observations of ozone vertical profiles and corresponding precursors in the low troposphere in Beijing, China. Atmos. Res. 213, 224–235. https://doi.org/10.1016/j.atmosres.2018.06.012.

Constantin, D.-E., Merlaud, A., Voiculescu, M., Van Roozendael, M., Arseni, M., Rosu, A., Georgescu, L., 2017. NO_2 and SO_2 observations in southeast Europe using mobile DOAS observations. Carpathian J. Earth Environ. Sci. 12 (2), 323–328. ISBN: 1842-4090.

Ding, X., He, Q., Shen, R., Yu, Q., Zhang, Y., Xin, J., Wen, T., Wang, X., 2016a. Spatial and seasonal variations of isoprene secondary organic aerosol in China: Significant impact of biomass burning during winter. Sci. Rep. 6, 20411. https://doi.org/10.1038/srep20411.

Ding, X., Zhang, Y., He, Q., Yu, Q., Shen, R., Zhang, Y., Zhang, Z., Lyu, S., Hu, Q., Wang, Y., Li, L., Song, W., Wang, X., 2016b. Spatial and seasonal variations of secondary organic aerosol from terpenoids over China. J. Geophys. Res.-Atmos. 121 (24), 14661–14678. https://doi.org/10.1002/2016JD025467.

Duncan, B.N., Yoshida, Y., Olson, J.R., Sillman, S., Martin, R.V., Lamsal, L., Hu, Y., Pickering, K.E., Retscher, C., Allen, D.J., Crawford, J.H., 2010. Application of OMI observations to a space-based indicator of NO_x and VOC controls on surface ozone formation. Atmos. Environ. 44 (18), 2213–2223. https://doi.org/10.1016/j.atmosenv.2010.03.010.

Fan, J., Ju, T., Wang, Q., Gao, H., Huang, R., Duan, J., 2021. Spatiotemporal variations and potential sources of tropospheric formaldehyde over eastern China based on

OMI satellite data. Atmos. Pollut. Res. 12 (1), 272–285. https://doi.org/10.1016/j.apr.2020.09.011.
Feng, Y., Ning, M., Lei, Y., Sun, Y., Liu, W., Wang, J., 2019. Defending blue sky in China: Effectiveness of the "Air Pollution Prevention and Control Action Plan" on air quality improvements from 2013 to 2017. J. Environ. Manage. 252, 109603 https://doi.org/10.1016/j.jenvman.2019.109603.
Fleischmann, O.C., Hartmann, M., Burrows, J.P., Orphal, J., 2004. New ultraviolet absorption cross-sections of bro at atmospheric temperatures measured by time-windowing fourier transform spectroscopy. J. Photochem. Photobiol. A Chem. 168 (1-2), 117–132. https://doi.org/10.1016/j.jphotochem.2004.03.026.
Friedfeld, S., Fraser, M., Ensor, K., Tribble, S., Rehle, D., Leleux, D., Tittelc, F., 2002. Statistical analysis of primary and secondary atmospheric formaldehyde. Atmos. Environ. 36 (30), 4767–4775. https://doi.org/10.1016/S1352-2310(02)00558-7.
Gao, C., Xiu, A., Zhang, X., Chen, W., Liu, Y., Zhao, H., Zhang, S., 2020. Spatiotemporal characteristics of ozone pollution and policy implications in Northeast China. Atmos. Pollut. Res. 11 (2), 357–369. https://doi.org/10.1016/j.apr.2019.11.008.
Gao, W., Tie, X., Xu, J., Huang, R., Mao, X., Zhou, G., Chang, L., 2017. Long-term trend of O_3 in a mega City (Shanghai), China: Characteristics, causes, and interactions with precursors. Sci. Total Environ. 603–604, 425–433. https://doi.org/10.1016/j.scitotenv.2017.06.099.
Garcia, A.R., Volkamer, R., Molina, L.T., Molina, M.J., Samuelson, J., Mellqvist, J., Galle, B., 2006. Separation of emitted and photochemical formaldehyde in Mexico City using a statistical analysis and a new pair of gas-phase tracers. Atmos. Chem. Phys. 6, 4545–4557. https://doi.org/10.5194/acp-6-4545-2006.
Gielen, C., Van Roozendael, M., Hendrick, F., Pinardi, G., Vlemmix, T., De Bock, V., De Backer, H., Fayt, C., Hermans, C., Gillotay, D., Wang, P., 2014. A simple and versatile cloud-screening method for MAX-DOAS retrievals. Atmos. Meas. Tech. 7, 3509–3527. https://doi.org/10.5194/amt-7-3509-2014.
Guo, P., Umarova, A.B., Luan, Y., 2020. The spatiotemporal characteristics of the air pollutants in China from 2015 to 2019. PLoS ONE 15 (8), e0227469. https://doi.org/10.1371/journal.pone.0227469.
Halla, J.D., Wagner, T., Beirle, S., Brook, J.R., Hayden, K.L., O'Brien, J.M., Ng, A., Majonis, D., Wenig, M.O., McLaren, R., 2011. Determination of tropospheric vertical columns of NO_2 and aerosol optical properties in a rural setting using MAX-DOAS. Atmos. Chem. Phys. 11 (253), 12475–12498. https://doi.org/10.5194/acp-11-12475-2011.
Hassan, S.K., El-Abssawy, A.A., Khoder, M.I., 2018. Effect of Seasonal Variation on the Levels and Behaviours of Formaldehyde in the Atmosphere of a Suburban Area in Cairo, Egypt. Asian J. Atmos. Environ. 12 (4), 356–368. https://doi.org/10.5572/ajae.2018.12.4.356.
Hönninger, G., Platt, U., 2002. Observations of BrO and its vertical distribution during surface ozone depletion at Alert. Atmos. Environ. 36, 2481–2490. https://doi.org/10.1016/S1352-2310(02)00104-8.
Ho, S.S.H., Ho, K.F., Lee, S.C., Cheng, Y., Yu, J.Z., Lam, K.M., Feng, N.S.Y., Huang, Y., 2012. Carbonyl emissions from vehicular exhausts sources in Hong Kong. J. Air Waste Manag. Assoc. 62 (2), 221–234. https://doi.org/10.1080/10473289.2011.642952.
Hong, Q., Liu, C., Hu, Q., Zhang, Y., Xing, C., Su, W., Ji, X., Xiao, S., 2021. Evaluating the feasibility of formaldehyde derived from hyperspectral remote sensing as a proxy for volatile organic compounds. Atmos. Res. 264 https://doi.org/10.1016/j.atmosres.2021.105777.
Hong, Q., Liu, C., Chan, K.L., Hu, Q., Xie, Z., Liu, H., Si, F., Liu, J., 2018. Ship-based MAX-DOAS measurements of tropospheric NO_2, SO_2, and HCHO distribution along the Yangtze River. Atmos. Chem. Phys. 18, 5931–5951. https://doi.org/10.5194/acp-18-5931-2018.
Huang, J., Pan, X., Guo, X., Li, G., 2018. Health impact of China's Air Pollution Prevention and Control Action Plan: an analysis of national air quality monitoring and mortality data. Lancet Planet. Health 2 (7), e313–e323. 10.1016-S2542-5196(18)30141-4.
Ibrahim, O., Platt, U., Shaiganfar, R., Wagner, T., 2010. Mobile MAX-DOAS observations of tropospheric trace gases. Atmos. Meas. Tech. 3, 129–140. https://doi.org/10.5194/amt-3-129-2010.
Javed, Z., Liu, C., Khokhar, M.F., Tan, W., Liu, H., Xing, C., Ji, X., Tanvir, A., Hong, Q., Sandhu, O., Rehman, A., 2019. Ground-Based MAX-DOAS Observations of CHOCHO and HCHO in Beijing and Baoding, China. Remote Sens. 11 (13), 1524. https://doi.org/10.3390/rs11131524.
Jiang, Z., Zheng, X., Zhai, H., Wang, Y., Wang, Q., Yang, Z., 2019. Seasonal and diurnal characteristics of carbonyls in the urban atmosphere of Changsha, a mountainous city in south-central China. Environ. Pollut. 253, 259–267. https://doi.org/10.1016/j.envpol.2019.06.127.
Jin, X., Fiore, A., Boersma, K.F., De Smedt, I., Valin, L., 2020. Inferring Changes in Summertime Surface Ozone-NO_x-VOC Chemistry over US Urban Areas from Two Decades of Satellite and Ground-Based Observations. Environ. Sci. Technol. 54, 6518–6529. https://doi.org/10.1021/acs.est.9b07785.
Khan, W.A., Khokhar, M.F., Shoaib, A., Nawaz, R., 2018. Monitoring and analysis of formaldehyde columns over Rawalpindi-Islamabad, Pakistan using MAX-DOAS and satellite observation. Atmos. Pollut. Res. 9 (5), 840–848. https://doi.org/10.1016/j.apr.2017.12.008.
Lamsal, L.N., Janz, S.J., Krotkov, N.A., Pickering, K.E., Spurr, R.J.D., Kowalewski, M.G., Loughner, C.P., Crawford, J.H., Swartz, W.H., Herman, J.R., 2017. High-resolution NO_2 observations from the Airborne Compact Atmospheric Mapper: Retrieval and validation. J. Geophys. Res. 122 (3), 1953–1970. https://doi.org/10.1002/2016JD025483.
Lee, C., Richter, A., Lee, H., Kim, Y.J., Burrows, J.P., Lee, Y.G., Choi, B.C., 2008. Impact of transport of sulfur dioxide from the Asian continent on the air quality over Korea during May 2005. Atmos. Environ. 42 (7), 1461–1475. https://doi.org/10.1016/j.atmosenv.2007.11.006.
Lei, W., Zavala, M., Foy, B.D., Volkamer, R., Molina, L.T., 2008. Impact of primary formaldehyde on air pollution in the Mexico City metropolitan area. Atmos. Chem. Phys. 8 (6), 19605–19635. https://doi.org/10.5194/acpd-8-19605-2008.
Li, M., Shao, M., Li, L.Y., Lu, S.H., Chen, W.T., Wang, C., 2014. Quantifying the ambient formaldehyde sources utilizing tracers. Chin. Chem. Lett. 25 (11), 1489–1491. https://doi.org/10.1016/j.cclet.2014.07.001.
Li, X., Brauers, T., Hofzumahaus, A., Lu, K., Li, Y.P., Shao, M., Wagner, T., Wahner, A., 2013. MAX-DOAS measurements of NO_2, HCHO and CHOCHO at a rural site in Southern China. Atmos. Chem. Phys. 13 (4), 2133–2151. https://doi.org/10.5194/acp-13-2133-2013.
Li, W., Shao, L., Wang, W., Li, H., Zhang, D., 2020a. Air quality improvement in response to intensified control strategies in Beijing during 2013–2019. Sci. Total Environ. 744, 140776 https://doi.org/10.1016/j.scitotenv.2020.140776.
Li, Y., Shao, M., Lu, S., Chang, C.-C., Dasgupta, P.K., 2010. Variations and sources of ambient formaldehyde for the 2008 Beijing Olympic games. Atmos. Environ. 44 (21–22), 2632–2639. https://doi.org/10.1016/j.atmosenv.2010.03.045.
Li, Y., Yin, S., Yu, S., Bai, L., Wang, X., Lu, X., Ma, S., 2021. Characteristics of ozone pollution and the sensitivity to precursors during early summer in central plain, China. J. Environ. Sci. 99, 354–368. https://doi.org/10.1016/j.jes.2020.06.021.
Li, Y., Yang, W., Xie, S., Wu, Y., 2020b. Estimations and uncertainty of biogenic volatile organic compound emission inventory in china for 2008–2018. Sci. Total Environ. 733 https://doi.org/10.1016/j.scitotenv.2020.139301.
Lin, Y.C., Schwab, J.J., Demerjian, K.L., Bae, M.-S., Chen, W.-N., Sun, Y., Zhang, Q., Hung, H.-M., Perry, J., 2012. Summertime formaldehyde observations in New York City: ambient levels, sources and its contribution to HOx radicals. J. Geophys. Res. Atmos. 117 (8) https://doi.org/10.1029/2011jd016504.
Ling, Z.H., Zhao, J., Fan, S.J., Wang, X.M., 2017. Sources of formaldehyde and their contributions to photochemical O_3 formation at an urban site in the Pearl River Delta, southern China. Chemosphere 168, 1293–1301. https://doi.org/10.1016/j.chemosphere.2016.11.140.
Liu, H., Liu, C., Xie, Z., Li, Y., Huang, X., Wang, S., Xu, J., Xie, P., 2017. A paradox for air pollution controlling in China revealed by "APEC Blue" and "Parade Blue". Sci. Rep. 6, 34408. https://doi.org/10.1038/srep34408.
Liu, R., Feng, T., Wang, S., Shi, C., Guo, Y., Nan, J., Deng, Y., Zhou, B., 2018. OMI satellite observed formaldehyde column from 2006 to 2015 over Xishuangbanna, southwest China, and validation using ground based zenith-sky DOAS. Sci. Total Environ. 613–614, 168–175. https://doi.org/10.1016/j.scitotenv.2017.08.210.
Liu, J., Li, X., Tan, Z., Wang, W., Yang, Y., Zhu, Y., Yang, S., Song, M., Chen, S., Wang, H., Lu, K., Zeng, L., Zhang, Y., 2021. Assessing the Ratios of Formaldehyde and Glyoxal to NO_2 as Indicators of O_3–NO_x–VOC Sensitivity. Environ. Sci. Technol. 55, 10935–10945. https://doi.org/10.1021/acs.est.0c07506.
Luecken, D.J., Hutzell, W.T., Strum, M.L., Pouliot, G.A., 2012. Regional sources of atmospheric formaldehyde and acetaldehyde, and implications for atmospheric modeling. Atmos. Environ. 47, 477–490. https://doi.org/10.1016/j.atmosenv.2011.10.005.
Lui, K.H., Ho, S.S.H., Louie, P.K.K., Chan, C.S., Lee, S.C., Hu, D., Chan, P.W., Lee, J.C.W., Ho, K.F., 2017. Seasonal behavior of carbonyls and source characterization of formaldehyde (HCHO) in ambient air. Atmos. Environ. 152, 51–60. https://doi.org/10.1016/j.atmosenv.2016.12.004.
Ma, Y., Diao, Y., Zhang, B., Wang, W., Ren, X., Yang, D., Wang, M., Shi, X., Zheng, J., 2016. Detection of formaldehyde emissions from an industrial zone in the Yangtze River Delta region of China using a proton transfer reaction ion-drift chemical ionization mass spectrometer. Atmos. Meas. Tech. 9 (12), 6101–6116. https://doi.org/10.5194/amt-9-6101-2016.
Ma, Z., Liu, C., Zhang, C., Liu, P., Ye, C., Xue, C., Zhao, D., Sun, J., Du, Y., Chai, F., Mu, Y., 2019. The levels, sources and reactivity of volatile organic compounds in a typical urban area of Northeast China. J. Environ. Sci. 79, 121–134. https://doi.org/10.1016/j.jes.2018.11.015.
Mahilang, M., Deb, M.K., Pervez, S., 2021. Biogenic secondary organic aerosols: A review on formation mechanism, analytical challenges and environmental impacts. Chemosphere 262, 127771. https://doi.org/10.1016/j.chemosphere.2020.127771.
Meller, R., Moortgat, c., 2000. Temperature dependence of the absorption cross sections of formaldehyde between 223 and 323 k in the wavelength range 225-375 nm. J. Geophys. Res. Atmos. 105 (D6), 7089–7101. https://doi.org/10.1029/1999JD901074.
Mhawish, A., Sorek-Hamer, M., Chatfield, R., Banerjee, T., Bilal, M., Kumar, M., Sarangi, C., Franklin, M., Chau, K., Garay, M., Kalashnikova, O., 2021. Aerosol characteristics from earth observation systems: A comprehensive investigation over South Asia (2000–2019). Remote Sens. Environ. 259 https://doi.org/10.1016/J.RSE.2021.112410.
Michel, V., Caroline, F., Francois, H., 2018. Centralised reprocessing of CINDI-2 MAX-DOAS slant column data sets. In: EGU General Assembly Conference Abstracts, p. 5252.
Nepita-Villanueva, M.R., Berlanga-Robles, C.A., Ruiz-Luna, A., Barcenas, J., 2019. Spatio-temporal mangrove canopy variation (2001–2016) assessed using the MODIS enhanced vegetation index (EVI). J. Coast. Conserv. 23 (3), 589–597. https://doi.org/10.1007/s11852-019-00689-9.
Nichol, J.E., Bilal, M., Ali, M.A., Qiu, Z., 2020. Air Pollution Scenario over China during COVID-19. Remote Sens. 12 (13) https://doi.org/10.3390/rs12132100.
Pang, X., Mu, Y., 2006. Atmos. Environ. 40 (33), 6313–6320. https://doi.org/10.1016/j.atmosenv.2006.05.044.
Paoletti, E., De Marco, A., Beddows, D.C., Harrison, R.M., Manning, W.J., 2014. Ozone levels in European and USA cities are increasing more than at rural sites, while peak

values are decreasing. Environ. Pollut. 192, 295–299. https://doi.org/10.1016/j.envpol.2014.04.040.

Possanzini, M., Di Palo, V., Cecinato, A., 2002. Sources and photodecomposition of formaldehyde and acetaldehyde in Rome ambient air. Atmos. Environ. 36 (19) https://doi.org/10.1016/S1352-2310(02)00192-9.

Rappengluck, B., Dasgupta, P.K., Leuchner, M., Li, Q., Luke, W., 2010. Formaldehyde and its relation to CO, PAN, and SO_2 in the Houston-Galveston airshed. Atmos. Chem. Phys. 10 (5), 2413–2424. https://doi.org/10.5194/acp-10-2413-2010.

Ryan, R.G., Rhodes, S., Tully, M., Wilson, S., Jones, N., Frieß, U., Schofield, R., 2018. Daytime HONO, NO_2 and aerosol distributions from MAX-DOAS observations in Melbourne. Atmos. Chem. Phys. 18 (19), 13969–13985. https://doi.org/10.5194/acp-18-13969-2018.

Sakamoto, Y., Sadanaga, Y., Li, Matsuoka, K., Takemura, M., Fujii, T., Nakagawa, M., Kohno, N., Nakashima, Y., Kei, Sato, Nakayama, T., Kato, S., Takami, A., Yoshino, A., Murano, K., Kajii, Y., 2019. Relative and Absolute Sensitivity Analysis on Ozone Production in Tsukuba, a City in Japan. Environ. Sci. Technol. 53 (23), 13629–13635. https://doi.org/10.1021/acs.est.9b03542.

Serdyuchenko, A., Gorshelev, V., Weber, M., Chehade, W., Burrows, J.P., 2014. High spectral resolution ozone absorption cross-sections-Part 2: temperature dependence. Atmos. Meas. Tech. 7, 625–636. https://doi.org/10.5194/amt-7-625-2014.

Shi, Y., Li, D.W., Chen, Y., He, X.Y., 2011. Emissions of Isoprenoid from Major Planting Tree Species in Shenyang. Adv. Mater. Res. 1154, 1041–1045. https://doi.org/10.4028/www.scientific.net/AMR.183-185.1041.

Sicard, P., De Marco, A., Troussier, F., Renou, C., Vas, N., Paoletti, E., 2013. Decrease in surface ozone concentrations at Mediterranean remote sites and increase in the cities. Atmos. Environ. 79, 705–715. https://doi.org/10.1016/j.atmosenv.2013.07.042.

Sicard, P., De Marco, A., Agathokleous, E., Feng, Z., Xu, X., Paoletti, E., Diéguez Rodriguez, J.J., Calatayud, V., 2020. Amplified ozone pollution in cities during the COVID-19 lockdown. Sci. Total Environ. 735 https://doi.org/10.1016/j.scitotenv.2020.139542.

Sindelarova, K., Markova, J., Simpson, D., Huszar, P., Karlicky, J., Darras, S., Granier, C., 2021. High resolution biogenic global emission inventory for the time period 2000–2019 for air quality modelling. Earth System Science Data Discussions. [preprint]. 10.5194/essd-2021-226, in review, 2021.

Sinreich, R., Frieß, U., Wagner, T., Platt, U., 2005. Multi axis differential optical absorption spectroscopy (MAX-DOAS) of gas and aerosol distributions. Faraday Discuss. 130, 153–164. https://doi.org/10.1039/b419274p.

Solomon, S., Schmeltekopf, A.L., 1987. On the Interpretation of Zenith Sky Absorption Measurements. J. Geophys. Res. Atmos. 92 (D7), 8311–8319. https://doi.org/10.1029/JD092iD07p08311.

Souri, A.H., Nowlan, C.R., Wolfe, G.M., Lamsal, L.N., Chan, M.C.E., Abad, G.G., Janz, S. J., Fried, A., Blake, D.R., Weinheimer, A.J., Diskin, G.S., Liu, X., Chance, K., 2020. Revisiting the effectiveness of $HCHO/NO_2$ ratios for inferring ozone sensitivity to its precursors using high resolution airborne remote sensing observations in a high ozone episode during the KORUS-AQ campaign. Atmos. Environ. 224 https://doi.org/10.1016/j.atmosenv.2020.117341.

Su, W., Liu, C., Hu, Q., Zhao, S., Sun, Y., Wang, W., Zhu, Y., Liu, J., Kim, J., 2019. Primary and secondary sources of ambient formaldehyde in the Yangtze River Delta based on Ozone Mapping and Profiler Suite (OMPS) observations. Atmos. Chem. Phys. 19 (10), 6717–6736. https://doi.org/10.5194/acp-19-6717-2019.

Sun, J., Shen, Z.X., Wang, R., Li, G., Cao, J., 2020. A comprehensive study on ozone pollution in a megacity in north china plain during summertime: observations, source attributions and ozone sensitivity. Environ. Int. 146, 106279 https://doi.org/10.1016/j.envint.2020.106279.

Sun, Y., Liu, H., Guo, Z., 2021. Capsule network-based approach for estimating grassland coverage using time series data from enhanced vegetation index. Artif. Intell. Geosci. 2, 26–34. https://doi.org/10.1016/J.AIIG.2021.08.001.

Tack, F., Merlaud, A., Iordache, M., Pinardi, G., Dimitropoulou, E., Eskes, H., Bomans, B., Veefkind, P., Van, R.M., 2021. Assessment of the TROPOMI tropospheric NO_2 product based on airborne APEX observations. Atmos. Meas. Tech. 4 (1), 615–646. https://doi.org/10.5194/AMT-14-615-2021.

Taguchi, S., Hagiwara, M., Shibata, A., Fujinari, H., Matsumoto, S., Kuwata, M., Sazawa, K., Hata, N., Kuramitz, H., 2021. Investigation and modeling of diurnal variation in suburban ambient formaldehyde concentration. Environ. Sci. Pollut. Res. 28 (11), 13425–13438. https://doi.org/10.1007/s11356-020-11465-w.

Thalman, R., Volkamer, R., 2013. Temperature dependent absorption cross-sections of O2-O2 collision pairs between 340 and 630 nm and at atmospherically relevant pressure. Phys. Chem. Chem. Phys. 15, 15371–15381. https://doi.org/10.1039/c3cp50968k.

Tian, J.Q., Fang, C.S., Qiu, J.X., Wang, J., 2020. Analysis of Pollution Characteristics and Influencing Factors of Main Pollutants in the Atmosphere of Shenyang City. Atmosphere 11. https://doi.org/10.3390/atmos11070766.

Wagner, T., Dix, B., Friedeburg, C.V., Frieß, U., Sanghavi, S., Sinreich, R., Platt, U., 2004. MAX-DOAS O_4 measurements: A new technique to derive information on atmospheric aerosols—Principles and information content. J. Geophys. Res.: Atmos. 109, D22205. https://doi.org/10.1029/2004JD004904.

Wagner, T., Beirle, S., Remmers, J., Shaiganfar, R., Wang, Y., 2016. Absolute calibration of the colour index and o-4 absorption derived from multi axis (max-) doas measurements and their application to a standardised cloud classification algorithm. Atmos. Meas. Tech. 9, 4803–4823. https://doi.org/10.5194/amt-2016-148.

Wang, C., Huang, X.-F., Han, Y., Zhu, B., He, L.-Y., 2017a. Sources and Potential Photochemical Roles of Formaldehyde in an Urban Atmosphere in South China. J. Geophys. Res.: Atmos. 122 (21), 11934–11947. https://doi.org/10.1002/2017JD027266.

Wang, T., Xue, L.K., Brimblecombe, P., Lam, Y.F., Li, L., Zhang, L., 2016. Ozone pollution in China: A review of concentrations, meteorological influences, chemical precursors, and effects. Sci. Total Environ. 575, 1582–1596. https://doi.org/10.1016/j.scitotenv.2016.10.081.

Wang, N., Lyu, X., Deng, X., Huang, X., Jiang, F., Ding, A., 2019. Aggravating O_3 pollution due to NO_x emission control in eastern China. Sci. Total Environ. 677, 732–744. https://doi.org/10.1016/j.scitotenv.2019.04.388.

Wang, P., 2021. China's air pollution policies: progress and challenges. Curr. Opin. Environ. Sci. Health 19, 100227. https://doi.org/10.1016/j.coesh.2020.100227.

Wang, W., Ronald, V., Ding, J., Weele, M.V., Cheng, T., 2021. Spatial and temporal changes of the ozone sensitivity in china based on satellite and ground-based observations. Atmos. Chem. Phys. 21 (9), 7253–7269. https://doi.org/10.5194/acp-21-7253-2021.

Wang, X., Wang, H., Wang, S., 2010. Ambient formaldehyde and its contributing factor to ozone and OH radical in a rural area. Atmos. Environ. 44 (17), 2074–2078. https://doi.org/10.1016/j.atmosenv.2010.03.023.

Wang, Y., Lampel, J., Xie, P., Beirle, S., Li, A., Wu, D., Wagner, T., 2017b. Ground-based MAX-DOAS observations of tropospheric aerosols, NO_2, SO_2 and HCHO in Wuxi, China, from 2011 to 2014. Atmos. Chem. Phys. 17 (3), 2189–2215. https://doi.org/10.5194/acp-17-2189-2017.

Wood, E.C., Canagaratna, M.R., Herndon, S.C., Onasch, T.B., Kolb, C.E., Worsnop, D.R., Kroll, J.H., Knighton, W.B., Seila, R., Zavala, M., Molina, L.T., DeCarlo, P.F., Jimenez, J.L., Weinheimer, A.J., Knapp, D.J., Jobson, B.T., Stutz, J., Kuster, W.C., Williams, E.J., 2010. Investigation of the correlation between odd oxygen and secondary organic aerosol in Mexico City and Houston. Atmos. Chem. Phys. 10 (18), 8947–8968. https://doi.org/10.5194/acp-10-8947-2010.

Xing, C., Liu, C., Hu, Q., Fu, Q., Lin, H., Wang, S., Su, W., Wang, W., Javed, Z., Liu, J., 2020. Identifying the wintertime sources of volatile organic compounds (VOCs) from MAX-DOAS measured formaldehyde and glyoxal in Chongqing, Southwest China. Sci. Total Environ. 715 https://doi.org/10.1016/j.scitotenv.2019.136258.

Xing, C., Liu, C., Hu, Q., Fu, Q., Wang, S., Lin, H., Zhu, Y., Wang, S., Wang, W., Javed, Z., Ji, X., Liu, J., 2021. Vertical distributions of wintertime atmospheric nitrogenous compounds and the corresponding OH radicals production in Leshan, Southwest China. J. Environ. Sci. 105, 44–55. https://doi.org/10.1016/j.jes.2020.11.019.

Xing, C., Liu, C., Wang, S., Chan, K.L., Gao, Y., Huang, X., Su, W., Zhang, C., Dong, Y., Fan, G., Zhang, T., Chen, Z., Hu, Q., Su, H., Xie, Z., Liu, J., 2017. Observations of the vertical distributions of summertime atmospheric pollutants and the corresponding ozone production in Shanghai, China. Atmos. Chem. Phys. 17 (23), 14275–14289. https://doi.org/10.5194/acp-17-14275-2017.

Xing, C., Liu, C., Wang, S., Hu, Q., Liu, H., Tan, W., Zhang, W., Li, B., Liu, J., 2019. A new method to determine the aerosol optical properties from multiple-wavelength O_4 absorptions by MAX-DOAS observation. Atmos. Meas. Tech. 12 (6), 3289–3302. https://doi.org/10.5194/amt-12-3289-2019.

Xu, J., Huang, X., Wang, N., Li, Y., Ding, A., 2021. Understanding ozone pollution in the Yangtze River Delta of eastern China from the perspective of diurnal cycles. Sci. Total Environ. 752 https://doi.org/10.1016/j.scitotenv.2020.141928.

Yang, Z., Cheng, H.R., Wang, Z.W., Peng, J., Zhu, J.X., Lyu, X.P., Guo, H., 2019. Chemical characteristics of atmospheric carbonyl compounds and source identification of formaldehyde in Wuhan, Central China. Atmos. Res. 228, 95–106. https://doi.org/10.1016/j.atmosres.2019.05.020.

Zara, M., Boersma, K.F., De Smedt, I., Richter, A., Peters, E., van Geffen, J.H.G.M., Beirle, S., Wagner, T., Van Roozendael, M., Marchenko, S., Lamsal, L.N., Eskes, H.J., 2018. Improved slant column density retrieval of nitrogen dioxide and formaldehyde for OMI and GOME-2A from QA4ECV: intercomparison, uncertainty characterisation, and trends. Atmos. Meas. Tech. 11 (7), 4033–4058. https://doi.org/10.5194/amt-11-4033-2018.

Zara M., Boersma K. F., Eskes H., Denier van der Gon H., Vilà-Guerau de Arellano J., Krol M., Swaluw E., Schuch W., Velders Guus J.M., 2021. Reductions in nitrogen oxides over the Netherlands between 2005 and 2018 observed from space and on the ground: Decreasing emissions and increasing O_3 indicate changing NOx chemistry. Atmos. Environ.: X, 9(prepublish) 10.1016/J.AEAOA.2021.100104.

Zhao, Y., Liu, K., Yu, Y., 2019. Relationship between $PM_{2.5}$ adsorption and leaf surface morphology in ten urban tree species in Shenyang, China. Energy Sources Part A: Recovery Utiliz. Environ. Effects 41 (8), 1029–1039. https://doi.org/10.1080/15567036.2018.1539136.

Zhang, C., Liu, C., Hu, Q., Cai, Z., Su, W., Xia, C., Zhu, Y., Wang, S., Liu, J., 2019. Satellite UV-Vis spectroscopy: implications for air quality trends and their driving forces in China during 2005–2017. Light Sci. Appl. 8 (1), 100. https://doi.org/10.1038/s41377-019-0210-6.

Ziemke, J.R., Chandra, S., Bhartia, P.K., 2001. "Cloud slicing": A new technique to derive upper tropospheric ozone from satellite measurements. J. Geophys. Res.: Atmos. 106 (D9), 9853–9867. https://doi.org/10.1029/2000JD900768.